photonics

MDPI

Article

Kramers–Kronig Transmission with a Crosstalk-Dependent Step Multiple-Input Multiple-Output Volterra Equalizer in a Seven-Core Fiber

Feng Tian [1,*], Tianze Wu [1], Chao Yu [2], Chuxuan Wang [3], Mohai Yue [1], Ran Gao [2], Qi Zhang [1], Zhipei Li [2], Qinghua Tian [1], Fu Wang [1] and Xiangjun Xin [1,2]

[1] State Key Laboratory of Information Photonics and Optical Communications, Beijing Key Laboratory of Space-Ground Interconnection and Convergence, School of Electronic Engineering, Beijing University of Posts and Telecommunications, Beijing 100876, China; wutianze@bupt.edu.cn (T.W.); buptymh@bupt.edu.cn (M.Y.); zhangqi@bupt.edu.cn (Q.Z.); tianqh@bupt.edu.cn (Q.T.); wangfu6672@gmail.com (F.W.); xjxin@bupt.edu.cn (X.X.)

[2] Advanced Research Institute of Multidisciplinary Science, Beijing Institute of Technology, Beijing 100081, China; yuchao@bit.edu.cn (C.Y.); 6120190142@bit.edu.cn (R.G.); lizhipei@bit.edu.cn (Z.L.)

[3] China Electronics Technology Group, Beijing 100041, China; wangchuxuan@bupt.edu.cn

* Correspondence: tianfeng@bupt.edu.cn

Abstract: In this paper, we experimentally demonstrate a net bit rate of 261.7 Gbit/s in a seven-core transmission system with a Kramers–Kronig (KK) receiver. The 10 GBaud 16-level quadrature amplitude modulation (QAM) signal is transmitted over a 2.5 km seven-core fiber, and the relationship between carrier-to-signal power ratio, signal power, frequency spacing, and optical power is analyzed. Moreover, a multiple-input multiple-output (MIMO) Volterra equalization algorithm with crosstalk-dependent steps is proposed to compensate for inter-core crosstalk and impairments induced by other devices. Compared to the single-input single-output (SISO) Volterra equalizer, the CSPR can be reduced by 1.3 dB, and the received power gain can reach up to 0.7 dB.

Keywords: crosstalk; Kramers–Kronig receiver; MIMO; optical fiber communication; seven-core transmission; Volterra equalizer

check for updates

Citation: Tian, F.; Wu, T.; Yu, C.; Wang, C.; Yue, M.; Gao, R.; Zhang, Q.; Li, Z.; Tian, Q.; Wang, F.; et al. Kramers–Kronig Transmission with a Crosstalk-Dependent Step Multiple-Input Multiple-Output Volterra Equalizer in a Seven-Core Fiber. *Photonics* **2023**, *10*, 1017. https://doi.org/10.3390/photonics10091017

Received: 24 April 2023
Revised: 13 August 2023
Accepted: 24 August 2023
Published: 5 September 2023

Copyright: © 2023 by the authors. Licensee MDPI, Basel, Switzerland. This article is an open access article distributed under the terms and conditions of the Creative Commons Attribution (CC BY) license (https://creativecommons.org/licenses/by/4.0/).

1. Introduction

With the popularity of 5G mobile communication and the promotion of the shift to online services due to the impact of COVID-19 in recent years, the demand for data centers and optical access networks with higher capacity has increased dramatically [1–3]. In the context of traditional single-mode fiber capacity gradually approaching the Shannon limit, space division multiplexing (SDM) is gradually becoming a research hotspot and inevitable trend in the future development of optical communications [4–12]. Uncoupled multicore fiber (UC-MCF) is a promising alternative to various SDM transmission media, and some high-capacity short- and medium-haul optical transmission and optical interconnections have been widely reported to increase the capacity of fiber-optic transmission systems [13,14]. It is demonstrated that a transmission capacity of 1.05 Pbit/s is obtained over a distance of 3 km using a 14-core hybrid multicore fiber in [15], transmitting 32QAM-OFDM in the single-mode core and QPSK in the few-mode core. The 37-core fiber is also used for short distance transmission, supporting 64- and 256-QAM signals with a capacity of 1.84 Pbit/s after 7.9 km transmission [16]. Multicore fibers offer significant potential for applications in short- and medium-range optical transmission due to their increased transmission bandwidth and interconnect density [17].

However, the multiple receivers are required in multicore optical transmission systems, which will increase the costs significantly. Especially, multiple coherent receivers are unable

to meet the short- and medium-range transmission and optical interconnection requirements due to their high cost, excessive power consumption, and large module size [18]. Meanwhile, single-sideband (SSB) modulation techniques based on intensity modulation and intensity detection (IM/DD) systems cannot overcome the signal impairment caused by frequency selective fading due to fiber chromatic dispersion [19]. The Kramers–Kronig (KK) receiver has been proposed in recent years as a potentially powerful technology to solve these problems [20,21]. The KK scheme eliminates signal-to-signal beat interference (SSBI) and overcomes the limitation that a single optical detector can only detect and process the intensity information of the optical signal. It reduces the carrier signal power ratio (CSPR) requirements and allows for the reconstruction of phase information from the light intensity using a single optical detector, provided that the signal meets the minimum phase conditions [22]. It has a bright future in short- and medium-range transmission scenarios using multicore fiber optic transmission systems due to its low cost and superior performance.

Meanwhile, a non-negligible problem with UC-MCF in the transmission is the inter-core crosstalk (XT) caused by field coupling between cores and the losses in each core. Recent researches for UC-MCF have shown that XT can ultimately limit transmission performance and system capacity while crosstalk is minimized in the design of multicore fibers [23]. The introduction of higher-order modulation signals into MCF transmissions can significantly improve spectral efficiency, while they are more susceptible to crosstalk. Moreover, the increasing number of cores also causes serious crosstalk. In SDM systems, the multiple-input multiple-output (MIMO) equalization algorithm is generally required to eliminate the effects of XT. For instance, an all-optical MIMO photonic integrated circuit in a mode division multiplexing (MDM) system is demonstrated in [24], successfully demultiplexing six modes after 30 km of few-mode fiber transmission. A real-time 6×6 MIMO-DSP is used in [25] to resist crosstalk in coupled-core multicore fiber (CC-MCF) transmission. The real-value 8×2 MIMO-DSP is also used for real-time transmission in a 48 km 10-mode MDM system [26]. The use of MIMO-DSP for crosstalk cancellation in UC-MCF transmission systems is demonstrated in [23,27]. The SDM transmission experiments typically employ linear MIMO equalization techniques to demultiplex spatial channels, while nonlinear MIMO schemes typically have superior performance [28]. For example, MIMO algorithms based on the Volterra series can be used to compensate the transceiver nonlinearity in SDM transmission system.

In this paper, an experimental demonstration of a 16-QAM signal with a net rate of 261.7 Gbit/s transmitted over a 2.5 km seven-core fiber with a KK receiver is investigated. The relationship between CSPR, signal power, frequency spacing, and received power is investigated in this seven-core fiber transmission system, and a point is identified where a balance is achieved between signal intensity and the KK receiver. In addition, we propose a MIMO Volterra equalizer with crosstalk-dependent steps to mitigate XT and nonlinear degradation. Compared with the single-input single-output Volterra (SISO-Volterra) equalizer, the gains of received power and CSPR can be up to 0.7 dB and 1.3 dB, respectively.

2. Principle of KK Transmission System

The transmit signal of the KK system is a SSB optical signal, i.e., the signal spectrum is on one side of the continuous wave (CW) tone. At the receiver, the KK algorithm reconstructs the full complex optical field information from the beating of signal with the CW tone by direct detection [29]. The premise of reconstructing the optical field is to satisfy the minimum phase condition [30], which means that the power of the CW tone is sufficiently high. We briefly review the essential algorithms of the KK receiver, and the details can be found in [20]. The optical field impinging upon the photodetector (PD) is expressed as

$$E(t) = E_s(t) + E_0(t)e^{i2\pi f_o t}(f_o \geq B/2), \quad (1)$$

where $E_s(t)$ represents the complex optical field of the signal, with the optical bandwidth of B. $E_0(t)$ represents a CW tone with amplitude $|E_0|$, which has a frequency approximating the center frequency of the signal. f_o is the frequency difference between the center frequency of the signal and the CW tone after the frequency shift, which we call the frequency interval. The current I produced by the PD is

$$I(t) = |E(t)|^2 = |E_s(t)|^2 + 2Re(E_s(t)E_0^*(t)e^{i2\pi f_o t}) + |E_0(t)|^2, \quad (2)$$

where the symbol (*) represents signal conjugation. Assuming that $|E_0|$ is large enough to ensure that the signal meets the minimum phase condition, the signal $E_s(t)$ can be reconstructed from the optical intensity $I(t)$ as

$$E_s(t) = \left\{ \sqrt{I(t)} e^{i\phi_e(t)} - E_0 \right\} e^{i2\pi f_o t} \quad (3)$$

$$\phi_e(t) = \frac{1}{2\pi} p.v. \int_{-\infty}^{\infty} \frac{log[I(t')]}{t - t'} dt'. \quad (4)$$

where $p.v.$ stands for Cauchy principal value.

In this paper, the scheme shown in Figure 1 is used to generate an SSB optical signal, and a tunable laser is exploited to generate the CW tones for reconstructing the optical field information by the KK algorithm described above. Experimentally, it is able to change and optimize the CSPR and frequency interval more easily by adjusting the tunable laser.

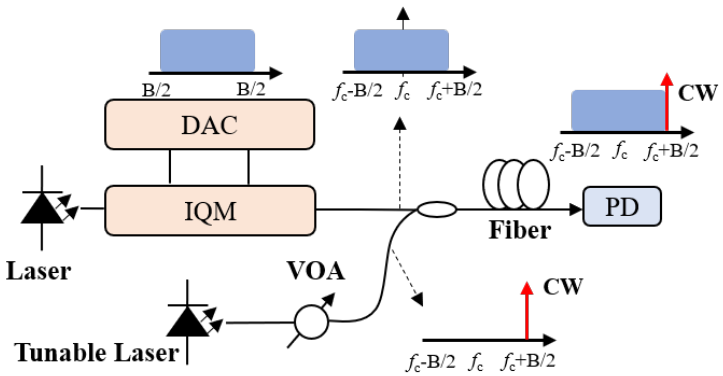

Figure 1. Scheme of SSB optical signal generation.

3. Experimental Setup and Analysis of Seven-Core Transmission System with KK Receiver

The experimental setup for the seven-core KK optical communication system is shown in Figure 2. CW is generated by the tunable laser source 1 (TLS1) with a linewidth of less than 100 kHz and output power less than 15 dBm. An I/Q modulator is then used to modulate the 10 GBaud 16-QAM signal with a 3 dB bandwidth of 33 GHz and an insertion loss of 6 dB. The signals are root-raised cosine (RRC) shaped with a roll-off of 0.2. An arbitrary waveform generator (AWG) of 64 GSa/s is used to convert two independent sequences of digital symbols into the electrical signals. An erbium-doped fiber amplifier (EDFA) with a noise figure of 5.5 dB and a variable optical attenuator (VOA) is used to adjust the signal launch power into a 1 × 2 coupler. The CW tone is generated by a TLS2 which can adjust the frequency. Another VOA adjusts the output power of carrier light, then coupled into the other side of the 1 × 2 coupler. The spectrum of the transmitted signal is shown in inset (i) of Figure 2. We use a 1 × 8 coupler and the delay lines for decorrelation of different channels and then couple the seven-channel signals into the seven-core fiber through fan-in and fan-out (FIFO) modules. A fiber delay of about 20 ns is applied to core2, core4, and core7, respectively, and a delay of about 30 ns is applied to core1, core3, core6. The inter-core skew with relation to the central core (core5) is measured to be −110 ps, −490 ps, 97 ps, 182 ps, −506 ps, 133 ps (core1→core7), and neighboring

cores can be effectively decorrelated. Table 1 shows the parameters of seven-core fiber and FIFO modules.

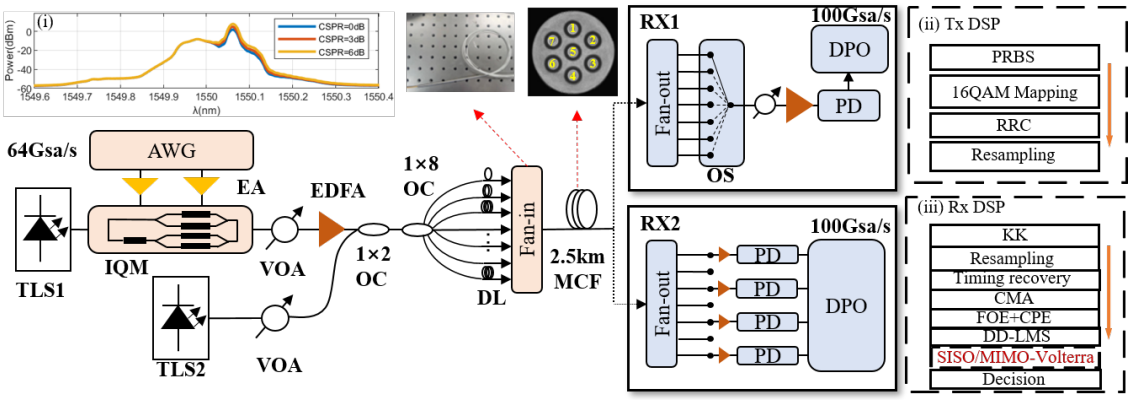

Figure 2. Experimental setup for the seven-core KK 16-QAM coherent optical communication system (TLS: tunable laser source; AWG: arbitrary waveform generator; IQM: I/Q modulator; EA: electric amplifier; OC: optical coupler; VOA: variable optical attenuator; DL: delay line; EDFA: erbium-doped fiber amplifier; OS: optical switch; PD: photodetector; DPO: digital phosphor oscilloscope). Inset (**i**) shows the spectrum of transmitted signals. Inset (**ii**,**iii**) show the transmitter and receiver DSP, respectively.

Table 1. Parameters and values of seven-core fiber and FIFO modules.

	Parameters	Values
Trench-assisted homogeneous seven-core fiber	Loss@1550 nm (dB/km)	0.25
	Mode field diameter@1550 nm (μm)	9.5
	Core layer diameter (μm)	7.9
	Core spacing (μm)	41.5 ± 1.5
	Cladding diameter (μm)	150 ± 2
FIFO modules	Maximum insertion loss (dB)	1.5

The transmission link is composed of 2.5 km seven-core optical fiber. Figure 3 shows the distributed crosstalk and crosstalk matrix in a seven-core fiber and FIFO. Figure 3a shows the temporal evolution of the crosstalk power with an average power of −45 dB generated by a CW light wave of 1550.13 nm within a 2.5 km 7-core MCF over 70 min, following the method in [6]. The measured core pairs are core4 and core5. The XT fluctuations are reduced when using amplified spontaneous emission (ASE) noise. Figure 3b shows the crosstalk matrix of the seven-core fiber with FIFO at a given time interval, using the continuous wave light emitted from one core, and the optical power of all cores is measured. The horizontal axis indicates the measured core label and the vertical axis denotes the input core label. The values in the cells of the figure are the decibels of energy transfer. The diagonal values of the matrix indicate the loss of each core. The maximum loss of core5 is 6.91 dB, and the minimum loss of core7 is 4.37 dB.

At the receiver, we adopt both RX1 and RX2 reception schemes. In the RX1, the signals are demultiplexed and selected using a fan-out module and an optical switch (OS). Behind the OS, a VOA and an EDFA with fixed gain are employed to adjust the received power. A four-channel digital phosphor oscilloscope (DPO) with a sampling rate of 100 GSa/s, a bandwidth of 20 GHz, and a 50-GHz PD is used to receive the signal. In the RX2, four channels are selected to receive with four PDs, and the signals are fed to the DPO simultaneously for MIMO equalization. The offline DSP includes the KK algorithm, resampling, the constant modulus algorithm (CMA) equalization, frequency offset estimation (FOE), carrier phase estimation (CPE), the decision-directed least mean square (DD-LMS) algorithm, the SISO/MIMO-Volterra algorithm, and bit error rate (BER) calculation.

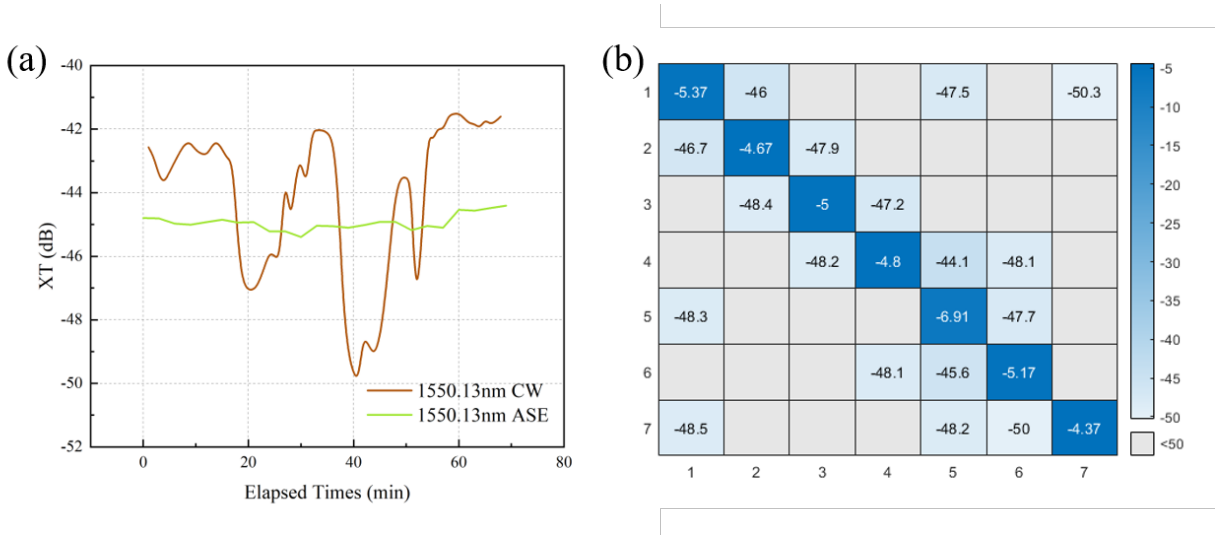

Figure 3. Distributed crosstalk (**a**) and crosstalk matrix (**b**) in seven-core fiber and FIFO modules.

We first analyze the performance of the seven-core transmission system using the reception scheme RX1. Figure 4 presents the BER values at different signal powers for the KK receiver when the carrier optical power is 10 dBm, where the dashed line represents the result of optical transmission with only one core in the link, i.e., there is no impact of XT; and the solid line represents the presence of XT. The performance gap between the dashed line and the solid line of the corresponding cores illustrates the impact of the above levels of crosstalk on signal performance. The transmission performance benefits from improving signal-to-noise ratio (SNR), with the signal power increasing from -8 dBm to 0 dBm. If the signal power increases to more than 0 dBm, fiber nonlinearity is improved and the quality of the KK receiver will decrease, which will lead to the decrease in the BER performance. When the signal power is further increased to 6 dBm, the BERs of core5 and core3 are 8.51×10^{-3} and 1.44×10^{-3}, respectively. In addition, the performance of the core varies due to diverse crosstalk levels and losses. It is noted that the performance gap between cores varies with signal power variations. It can be seen that from -6 dBm to 6 dBm, the performance difference between the cores for high signal power is greater than the performance difference for low signal power. From Figure 4, it can be predicted that for low power, the minimum power (core2) and maximum power (core5) for each core to reach below the FEC threshold are -8 dBm and -6 dBm, respectively. In contrast, for the high power, the minimum power (core5) and maximum power (core7) for each core to return above the FEC threshold are 5 dBm and exceed 10 dBm, respectively. Meanwhile, the performance difference between cores with XT at high signal power is greater than without XT. The curves of all cores without XT tend to converge at high signal power, while the curves with XT are divergent. We predict that the crosstalk produced at low power is drowned out by the amplifier noise. The effect of XT is suppressed, whereas the impact of crosstalk at high power becomes significant. Furthermore, high signal power leads to stronger fiber nonlinearity, which interacts with crosstalk to compromise the performance of the SISO-Volterra equalizer, which makes the degradation of the BER is greater than the effect of the XT. Since core5 is the middle core, it is affected by crosstalk between cores the most, which is consistent with the results in Figure 4 and our conclusion.

Figure 5 describes the relationship between BER and CSPR when the signal power is 0 dBm. With the CSPR increasing from 3 dB to 13 dB, the BER of core7 decreases from 5.70×10^{-3} to 9.46×10^{-5}, respectively. The maximum penalty of CSPR is 2.1 dB at the HD-FEC threshold (3.8×10^{-3}) because the crosstalk between core5 and core7 are different.

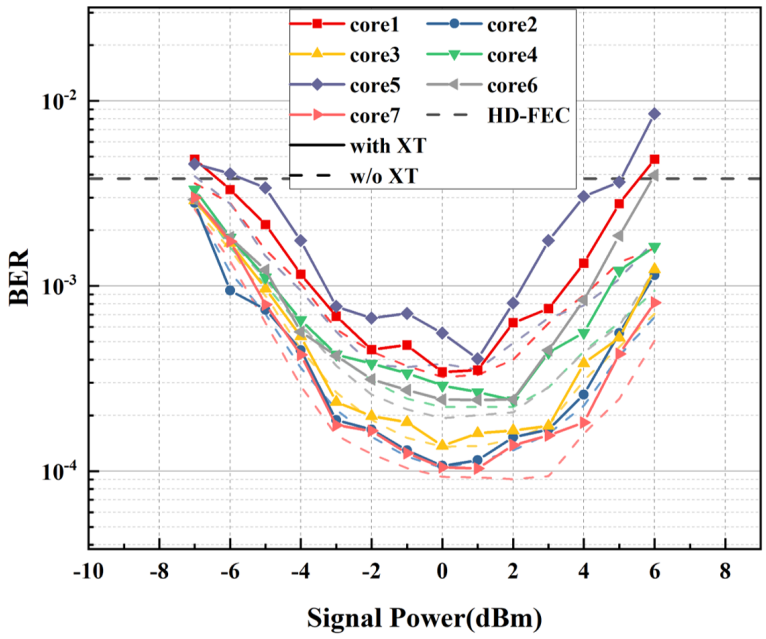

Figure 4. BER versus signal power when carrier power is 10 dBm.

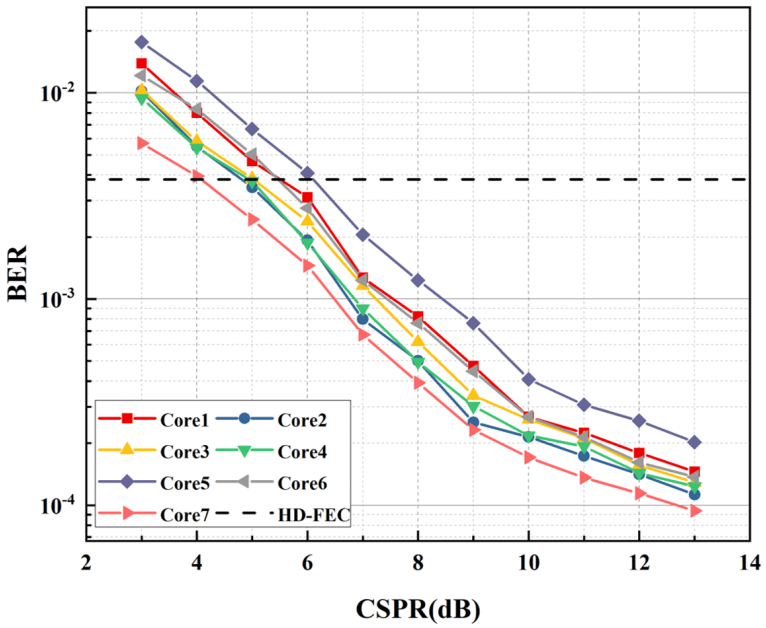

Figure 5. BER as a function of CSPR when signal power is 0 dBm.

Figure 6 shows the relationship between BER and frequency interval when signal power is 0 dBm, and CSPR is 10 dB. The bandwidth is 6 GHz when the RRC roll-off factor is 0.2. The signal power and the carrier power will be mixed, and the direct current (DC) component and the signal cannot be decoded when the frequency interval is less than 5 GHz. The BER decreases when the frequency interval increases from 5.625 GHz to 11.25 GHz. The BER values of core5 and core7 are 3.89×10^{-4} and 7.62×10^{-5} at a frequency interval of 11.25 GHz, respectively. The BER increases from 7.62×10^{-5} to 6.69×10^{-3} due to the actual bandwidth limit of the oscilloscope when the frequency interval increases from 11.25 GHz to 13.75 GHz.

Figure 7 shows the relationship between BER and the received power when the signal power is 0 dBm, and the CSPR is 10 dB. The BER will decrease from 8.87×10^{-2} to 6.68×10^{-5} when the received power is from 0 dBm to 7 dBm. The maximum penalty of received power is 1.2 dB at the HD-FEC threshold. The line rate of the system is 280 Gbits/s

(7 × 10 GBaud × 4 bits/symbol). Taking into account the 7% FEC overhead, the system has a net bit rate of 261.7 Gbits/s.

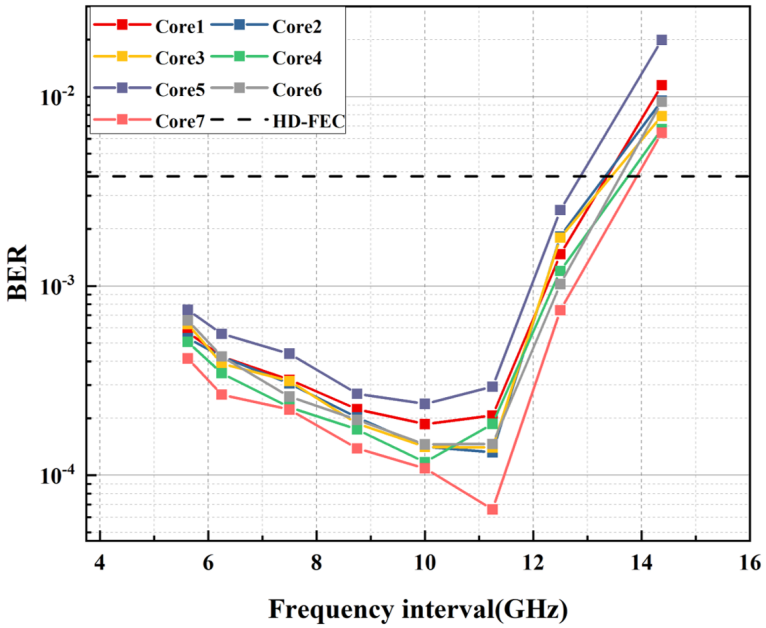

Figure 6. BER as a function of frequency interval when carrier power is 10 dBm and the signal power is 0 dBm.

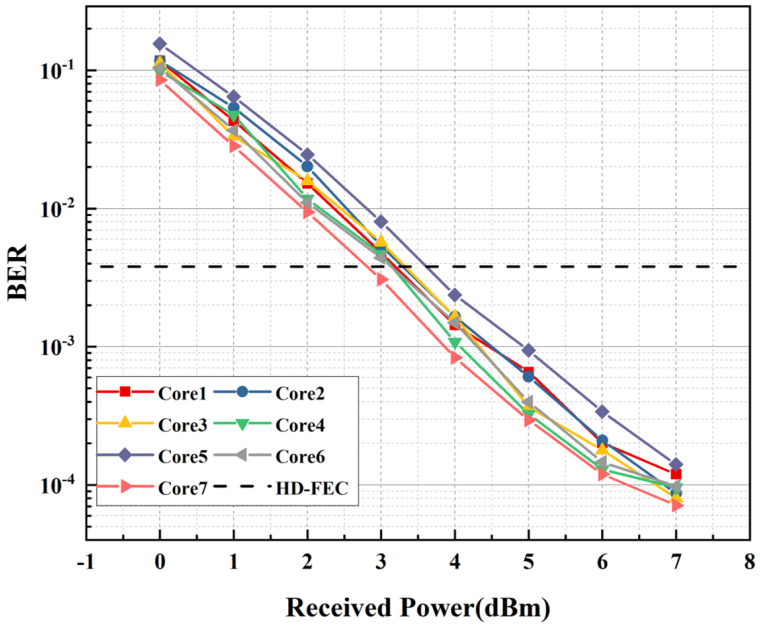

Figure 7. BER as a function of frequency interval when carrier power is 10 dBm and the signal power is 0 dBm.

4. XT-MIMO Nonlinear Equalization Algorithm Based on Volterra Series

A MIMO-Volterra equalization algorithm is proposed for compensating the nonlinear impairments, the power impairments, and XT in multicore fiber transmission systems. In multicore fibers, the coupling effects between modes in adjacent cores lead to XT, which limit the capacity and transmission distance of the system. The input and output of the multicore system are a complex nonlinear relationship due to the combined effects of the XT in the multicore optical fiber and the nonlinear impairment of the devices [31–33]. To solve the problem of the nonlinear effects, the Volterra series can extract the nonlinear

impairment characteristics of the device and the probability model of the nonlinear system. The Volterra series provides a complete description of the nonlinear impairments caused by devices such as electrical amplifiers, I/Q modulators, and PDs in the system.

The input–output relationship of the third-order limited-band Volterra model for the i-th fiber core can be expressed as

$$\begin{aligned} y_i'(n) &= \sum_{p=0}^{L_1} h^{(1)}(p)x_i(n-p) + \sum_{p=0}^{L_2}\sum_{q=p}^{L_2} h^{(2)}(p,q)x_i(n-p)x_i(n-q) \\ &+ \sum_{p=0}^{L_3}\sum_{q=p}^{L_3}\sum_{l=q}^{L_3} h^{(3)}(p,q,l)x_i(n-p)x_i(n-q)x_i^*(n-l). \end{aligned} \tag{5}$$

where $x_i(n)$ and $y_i'(n)$ are the input and output symbols of the i-th core, respectively. n is the index of signals. L_j is the memory length of the j-th order; $h^{(j)}$ is the j-th kernel of the Volterra filter. The first term of (5) represents a linear filter, while the other terms represent nonlinear terms. In the fiber optic transmission system, the second-order nonlinear memory length is 0, and only the first and third terms are considered. Then, the XT and nonlinearity of the MCF system can be represented by a nonlinear MIMO channel based on the Volterra series, and the input–output relationship of the MCF system can be expressed as

$$\begin{bmatrix} y_1(k) \\ y_2(k) \\ \cdots \\ y_m(k) \end{bmatrix} = \begin{bmatrix} C_{11}(k) & C_{21}(k) & \cdots & C_{m1}(k) \\ C_{12}(k) & C_{22}(k) & & C_{m2}(k) \\ \cdots & & \cdots & \\ C_{1m}(k) & C_{2m}(k) & & C_{mm}(k) \end{bmatrix} \begin{bmatrix} y_1'(k) \\ y_2'(k) \\ \cdots \\ y_m'(k) \end{bmatrix}. \tag{6}$$

where $y_i(k)$ denotes the k-th output symbol of the i-th core of the MCF system; $C_{ij}(k)$ $(i, j = 1, 2, \ldots, m)$ is the signal crosstalk coefficient of k-th time interval. m represents the index of cores.

In this paper, the nonlinear MIMO equalization algorithm based on the Volterra series and the characteristic coefficient of XT is proposed to compensate for linear crosstalk and nonlinear impairments in space division multiplexed systems. The MIMO-Volterra equalizer consists of linear equalization branches and nonlinear equalization branches, which are completed by the first-order and third-order terms of the Volterra equalizer. The block diagram of the equalizer is shown in Figure 8. The MIMO nonlinear equalization scheme based on the Volterra series improves the noise tolerance of multicore fiber transmission systems. Figure 9 shows the diagram of the XT-MIMO-Volterra nonlinear equalization algorithm. The specific algorithm flow is as follows.

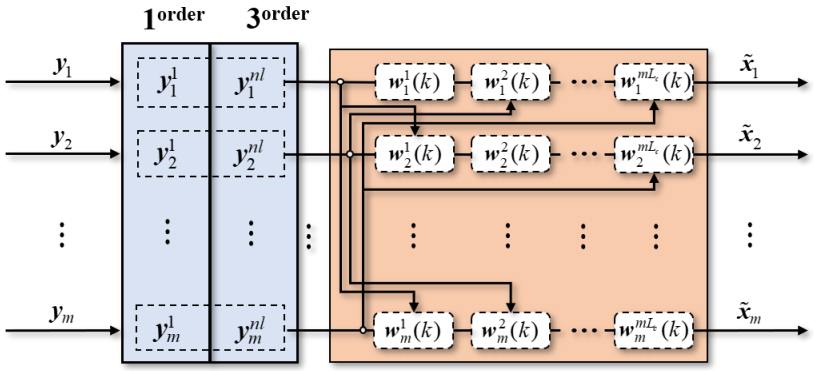

Figure 8. Block diagram of the first-order and third-order MIMO-Volterra equalizers.

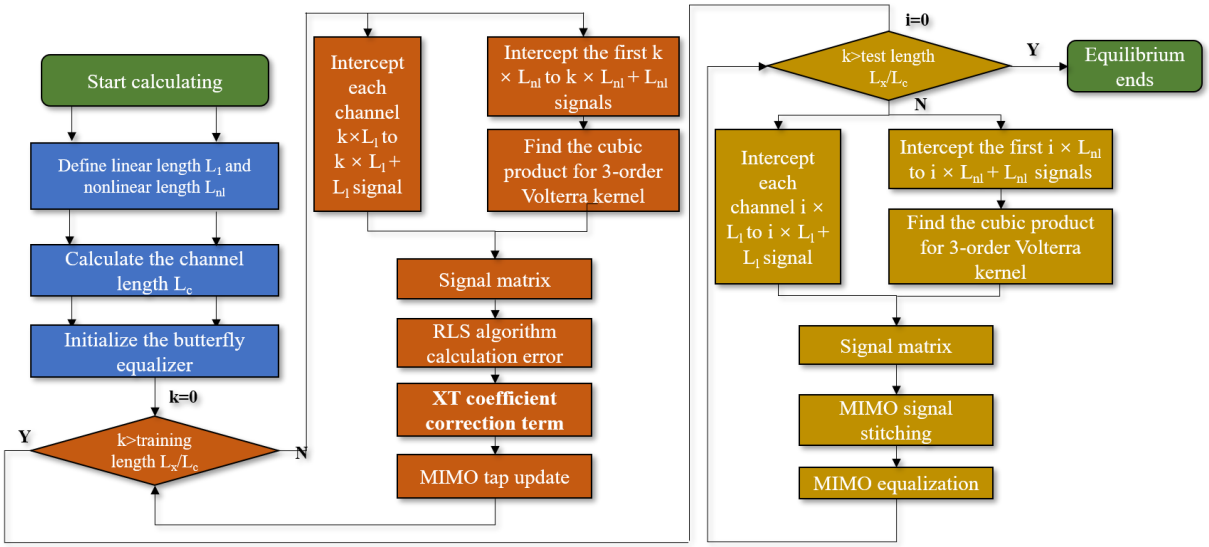

Figure 9. Flow diagram of the XT-MIMO nonlinear equalization algorithm based on the Volterra series.

1. Assume that the 16-QAM signal data matrix for all cores input to the equalizer is represented as

$$\boldsymbol{D} = \begin{bmatrix} y_1(1) & y_1(2) & \dots & y_1(n) \\ y_2(1) & y_2(2) & \dots & y_2(n) \\ \dots & \dots & \dots & \dots \\ y_m(1) & y_m(2) & \dots & y_m(n) \end{bmatrix} = \begin{bmatrix} \boldsymbol{y}_1 \\ \boldsymbol{y}_2 \\ \dots \\ \boldsymbol{y}_m \end{bmatrix}. \tag{7}$$

where $y_m(n)$ represents signal and each channel includes the training signal and the payload signal.

2. Calculate the third-order nonlinear length as

$$\begin{aligned} L_{nl} &= \sum_{v_3=v_1}^{L_3} \sum_{v_2=v_3}^{L_3} \sum_{v_1=1}^{L_3} \\ &= \frac{1}{12}[3L_3(L_3+1) + L_3(L_3+1)(2L_3+1)]. \end{aligned} \tag{8}$$

3. Calculate the total channel length as

$$L_c = L_1 + L_{nl}. \tag{9}$$

4. Initialize the butterfly equalizer, and the tap coefficient of the equalizer can be expressed as

$$\boldsymbol{w}(k) = \begin{bmatrix} w_1^0(k) & w_2^0(k) & \dots & w_m^0(k) \\ w_1^1(k) & w_2^1(k) & \dots & w_m^1(k) \\ \dots & \dots & \dots & \dots \\ w_1^{mL_c}(k) & w_2^{mL_c}(k) & \dots & w_m^{mL_c}(k) \end{bmatrix} = \begin{bmatrix} \boldsymbol{w}_{11}(k) & \boldsymbol{w}_{12}(k) & \dots & \boldsymbol{w}_{1m}(k) \\ \boldsymbol{w}_{21}(k) & \boldsymbol{w}_{22}(k) & \dots & \boldsymbol{w}_{2m}(k) \\ \dots & \dots & \dots & \dots \\ \boldsymbol{w}_{m1}(k) & \boldsymbol{w}_{m2}(k) & \dots & \boldsymbol{w}_{mm}(k) \end{bmatrix}. \tag{10}$$

Let $w_i^{\lceil H_1 \rceil}(0)(i = 1, 2, \dots, m)$ is 1, where $H_1 = \frac{L_1}{2}$ and the other terms of $\boldsymbol{w}(0)$ are 0. $\boldsymbol{w}_{ij}(k)(i, j = 1, 2, ..., m)$ is a column vector of length L_c.

5. Intercept the $(k+1)\lceil H_1 \rceil - \lfloor H_1 \rfloor$ to $(k+1)\lceil H_1 \rceil + \lfloor H_1 \rfloor$ signals of each core from $k = 1$ and arrange them in reverse order to obtain the linear input sequence of the equalizer for each channel as

$$\boldsymbol{y}_i^1(k) = \begin{bmatrix} y_i((k+1)\lceil H_1 \rceil + \lfloor H_1 \rfloor) \\ \cdots \\ y_i((k+1)\lceil H_1 \rceil - \lfloor H_1 \rfloor) \end{bmatrix}. \tag{11}$$

Intercept the signals from $(k+1)\lceil H_1 \rceil - \lfloor H_3 \rfloor$ to $(k+1)\lceil H_3 \rceil + \lfloor H_3 \rfloor$ of each core and arrange them in reverse order, using (12) to find the cubic product of the input signals corresponding to the third-order Volterra kernel for each channel.

$$\boldsymbol{y}_i^{nl}(k) = \begin{bmatrix} y_i(A)y_i(A)y_i(A) \\ \cdots \\ y_i(A-v_3)y_i(A-v_2)y_i(A-v_1) \\ \cdots \\ y_i(B)y_i(B)y_i(B) \end{bmatrix}, \tag{12}$$

where

$$A = (k+1)\lceil H_3 \rceil + \lfloor H_3 \rfloor$$
$$B = (k+1)\lceil H_3 \rceil - \lfloor H_3 \rfloor.$$

6. Splice the linear sequence with a third order to obtain the input sequence for each channel, shown as

$$\boldsymbol{y}_i(k) = \begin{bmatrix} \boldsymbol{y}_i^1(k) \\ \boldsymbol{y}_i^{nl}(k) \end{bmatrix}. \tag{13}$$

7. Splice the MIMO equalizer input sequence of each channel into a MIMO input sequence, as shown in (14).

$$\boldsymbol{y}(k) = \begin{bmatrix} \boldsymbol{y}_1(k) & \boldsymbol{y}_2(k) & \cdots & \boldsymbol{y}_m(k) \\ \boldsymbol{y}_2(k) & \boldsymbol{y}_1(k) & \cdots & \boldsymbol{y}_1(k) \\ \cdots & \cdots & \cdots & \cdots \\ \boldsymbol{y}_m(k) & \boldsymbol{y}_m(k) & \cdots & \boldsymbol{y}_{m-1}(k) \end{bmatrix} \tag{14}$$

8. Calculate the MIMO output signal as

$$\tilde{\boldsymbol{x}}(k) = \boldsymbol{w}^T(k-1)\boldsymbol{y}(k) = \begin{bmatrix} \tilde{x}_1(k) \\ \tilde{x}_2(k) \\ \cdots \\ \tilde{x}_m(k) \end{bmatrix}. \tag{15}$$

9. Calculate the error as

$$\boldsymbol{\varepsilon}(k) = \boldsymbol{d}(k) - \tilde{\boldsymbol{x}}(k) = \begin{bmatrix} \varepsilon_1(k) \\ \varepsilon_2(k) \\ \cdots \\ \varepsilon_m(k) \end{bmatrix}. \tag{16}$$

where $\boldsymbol{d}(k)$ is the corresponding original signal.

10. Update the inverse of the correlation matrix as [34]:

$$\mathbf{R}_{D,i}^{-1}(k) = \frac{1}{\lambda}[\mathbf{R}_{D,i}^{-1}(k-1) - \frac{\mathbf{R}_{D,i}^{-1}(k-1)\mathbf{y}_i(k)\mathbf{y}_i^T(k)\mathbf{R}_{D,i}^{-1}(k-1)}{\lambda + \mathbf{y}_i^T(k)\mathbf{R}_{D,i}^{-1}(k-1)\mathbf{y}_i(k)}]. \quad (17)$$

where $\mathbf{R}_{D,i}^{-1}(k)(i = 1, 2, ..., m)$ is the inverse of the correlation matrix, and $\mathbf{R}_{D,i}^{-1}(0)$ is initialized to a unit matrix. $0 < \lambda \leq 1$ is called the forgetting factor, which has some forgetting effect on historical data. In this paper, $\lambda = 1$, which means no forgetting effect.

11. Calculate the crosstalk coefficient matrix according to the measured crosstalk matrix as

$$\boldsymbol{XT}_{opt}(k) = \begin{bmatrix} XT_{opt,11}(k) & XT_{opt,12}(k) & \dots & XT_{opt,1m}(k) \\ XT_{opt,21}(k) & XT_{opt,22}(k) & \dots & XT_{opt,2m}(k) \\ \dots & \dots & \dots & \dots \\ XT_{opt,m1}(k) & XT_{opt,m2}(k) & \dots & XT_{opt,mm}(k) \end{bmatrix}, \quad (18)$$

where

$$XT_{opt,ij}(k) = \rho\frac{XT_{ij}(k) - XT_{min}(k)}{XT_{max}(k) - XT_{min}(k)}(i, j = 1, 2, ..., m). \quad (19)$$

$XT_{ij}(k)$ represents the value of the measured crosstalk level of k-th time interval, $XT_{max}(k)$ and $XT_{min}(k)$ are the maximum and minimum values in the crosstalk matrix, respectively. ρ is the scaling factor. For example, in Figure 3b, $XT_{12}(k) = 10^{-46.7/10}$, $XT_{max}(k) = 10^{-4.67/10}$ and $XT_{min}(k) = 10^{-50.3/10}$, which is negligible for less than -50 dB (gray cells in the crosstalk matrix) , corresponding to $XT_{opt,ij}(k)$ of 0. Since the inter-core XT changes relatively slowly, the crosstalk matrix is collected once in one minute. We use the average crosstalk power in one minute for the calculation of the algorithm crosstalk coefficient, i.e., $XT_{ij}(1) = XT_{ij}(2) = ... = XT_{ij}(k)$. The transmitted signal is processed with the crosstalk matrix in the corresponding time interval. Considering that $\boldsymbol{XT}_{opt}(k)$ is a singular matrix, the inverse matrix of $\boldsymbol{XT}_{opt}(k)$ is

$$\boldsymbol{XT}_{opt}^{-1}(k) = \begin{bmatrix} XT_{opt,11}^{'}(k) & XT_{opt,12}^{'}(k) & \dots & XT_{opt,1m}^{'}(k) \\ XT_{opt,21}^{'}(k) & XT_{opt,22}^{'}(k) & \dots & XT_{opt,2m}^{'}(k) \\ \dots & \dots & \dots & \dots \\ XT_{opt,m1}^{'}(k) & XT_{opt,m2}^{'}(k) & \dots & XT_{opt,mm}^{'}(k) \end{bmatrix}, \quad (20)$$

12. Update the tap coefficient of the equalizer using (20) and (21):

$$\boldsymbol{w}_{ij}(k) = \boldsymbol{w}_{ij}(k-1) + XT_{opt,ij}^{'}\frac{\boldsymbol{R}_{D,i}^{-1}(k-1)\boldsymbol{y}_i(k)}{\lambda + \boldsymbol{y}_i^T(k)\boldsymbol{R}_{D,i}^{-1}(k-1)\boldsymbol{y}_i(k)}\boldsymbol{\varepsilon}_i(k). \quad (21)$$

See Appendix A for a detailed explanation of the derivation process.

13. Repeat steps 5 to steps 12 until the end of the training signal is updated and converged.
14. Extract the payload signal and repeat steps 5 to steps 8 until the end of the payload signal is updated, and complete the MIMO equalization.

5. Experimental Results and Performance Analysis of XT-MIMO Nonlinear Equalization

Figure 10a shows the constellation diagram of the signal. The signal mainly suffers from the nonlinear impairment of the device including the FIFO modules and the influence of crosstalk in the transmission link. The first- and third-order memory lengths of Volterra filters are optimized to 21 and 5, respectively. The performance of the signal improved after adopting the SISO-Volterra algorithm, MIMO-Volterra algorithm, and XT-MIMO-

Volterra algorithm, respectively. Figure 10b shows the mean square error (MSE) curve of the signal. The peaks of the MSE after passing through the SISO-Volterra algorithm, the MIMO-Volterra algorithm, and the XT-MIMO-Volterra algorithm are 6, 2.7, and 1.6, respectively. It can be seen that the MIMO-Volterra algorithm can effectively suppress the signal impairments, and the XT-MIMO-Volterra algorithm shows the best performance for equalizing the signal impairments compared with two other algorithms.

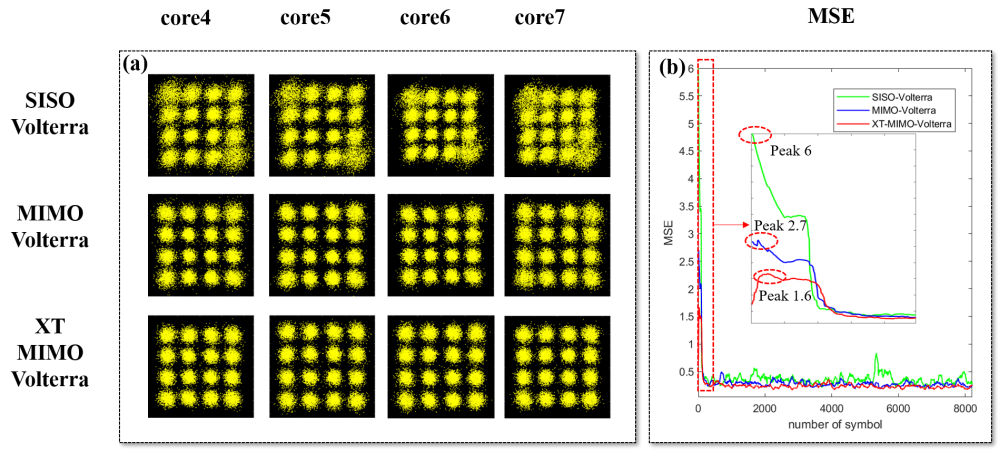

Figure 10. Experimental results: (**a**) the constellation diagram and (**b**) the mean square error curve of the signal after passing through the SISO-Volterra algorithm, the MIMO-Volterra algorithm, and the XT-MIMO-Volterra algorithm, respectively.

Figure 11 shows the experimental results for the seven-core transmission system with the KK receiver. Linear coordinates are employed for the y-axis in Figure 11a, and logarithmic coordinates are used in Figure 11b–d to enhance readability. Figure 11a shows the relationship between BER and signal power when the carrier optical power is 10 dBm. The observed signal power ranges from -7 dBm to 6 dBm, and the BER decreases with the increasing signal power in the range of -7 dBm $\sim$ 0 dBm. As the signal power increases from 0 dBm to 6 dBm, the BER performance will be worse, which is mainly affected by the CSPR and the quality of the KK receiver. For low CSPR, BER performance is more significantly improved by the MIMO-Volterra equalizer. For instance, the BER of MIMO-Volterra and XT-MIMO-Volterra are both below the FEC threshold when the signal power increases beyond 0 dBm, while w/o Volterra and SISO-Volterra are above the FEC threshold at 5.2 dBm and 5.7 dBm, respectively. There is little correlation between the difference in performance of cores and algorithms. Therefore, the average BER of the four channels (core4, core5, core6, and core7) is used to clearly compare the performances between different algorithms in Figure 11b–d.

The signal power is set at 0 dBm in Figure 11b. The measured CSPR varies in the range of 3 dB and 13 dB. When the CSPR is greater than 13 dB, the optical power exceeds the normal operating range of the seven-core fan-in module. As the CSPR rises, the XT-MIMO-Volterra algorithm will show the optimal performance. When the HD-FEC threshold is achieved, the CSPRs of w/o Volterra, SISO-Volterra, MIMO-Volterra, and XT-MIMO-Volterra are 6.5 dB, 5.4 dB, 4.8 dB, and 4.1 dB, respectively. Compared with MIMO-Volterra and SISO-Volterra, the XT-MIMO-Volterra algorithm can reduce the CSPR by 0.7 dB and 1.3 dB, respectively.

In Figure 11c, the carrier optical power is fixed to 10 dBm and the observed frequency interval range is 5.625 GHz to 14.375 GHz. The 10 GBaud signal and carrier are aliased and cannot be demodulated typically when the frequency interval is less than 5 GHz. The performance decreases with the increase in the frequency interval from 5.625 GHz to 11.25 GHz. For frequency interval = 11.25 GHz, the BERs of w/o Volterra, SISO-Volterra, MIMO-Volterra, and XT-MIMO-Volterra are 4.88×10^{-4}, 3.55×10^{-4}, 2.14×10^{-4}, and 1.36×10^{-4}, respectively. As the frequency spacing increases from 11.25 GHz to 14.375 GHz,

the BER performance degrades with the frequency spacing due to the 3-dB bandwidth of the oscilloscope is 20 GHz, which limits the performance.

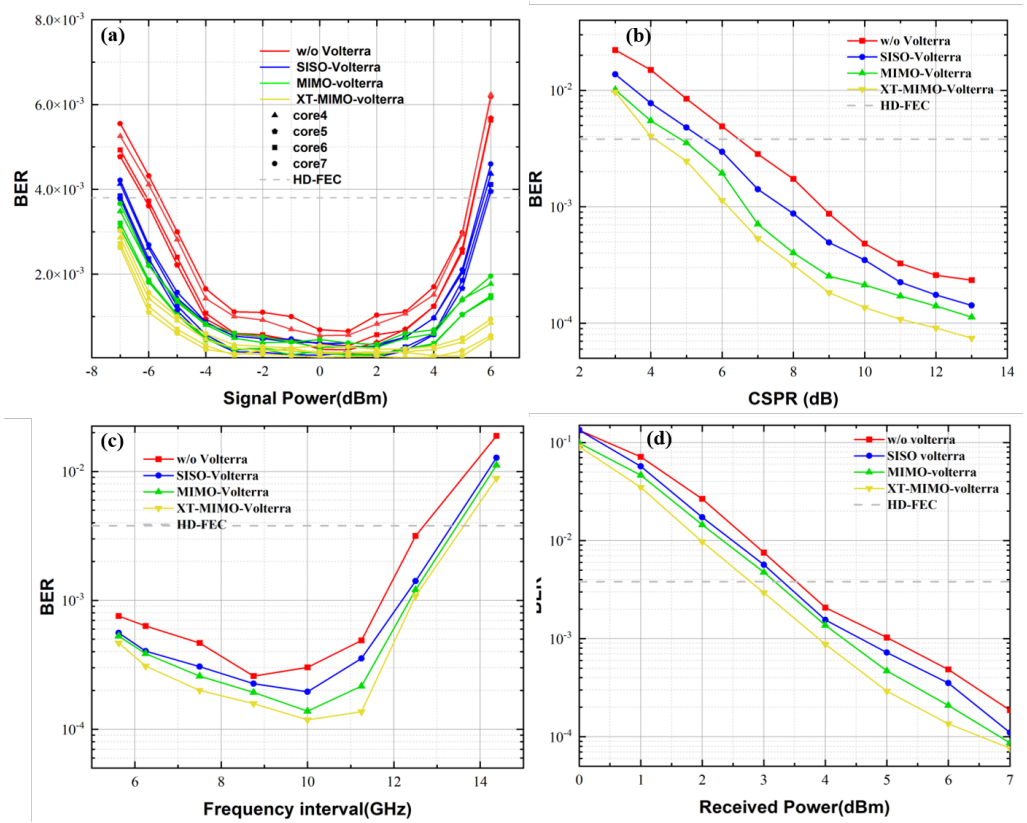

Figure 11. Experimental results. (**a**) BER as a function of signal power when the carrier power is 10 dBm, (**b**) BER as a function of CSPR when the carrier power is 10 dBm, (**c**) the relationship between BER with frequency interval (**c**) and received power (**d**), respectively.

Figure 11d shows the relationship between BER and received power for a signal power of 0 dBm and a carrier optical power of 10 dBm. The received power in the seven-core experimental system with KK receiver is from 0 dBm to 7 dBm, and the BER decreases with the increase in CSPR. For the received power = 7 dBm, the BERs of w/o Volterra, SISO-Volterra, MIMO-Volterra, and XT-MIMO-Volterra are 1.83×10^{-4}, 1.09×10^{-4}, 9.15×10^{-5} and 7.62×10^{-5}, respectively. The HD-FEC threshold can be achieved when the received power is 3.5 dBm to 7 dBm. At the HD-FEC threshold, the gain of the XT-MIMO-Volterra algorithm improved by 0.5 dB and 0.7 dB compared with the MIMO-Volterra and SISO-Volterra algorithms, respectively.

6. Conclusions and Discussion

In this paper, the experiment of a 261.7 Gbit/s 16-QAM signal transmitting a 2.5 km seven-core fiber with a KK receiver was demonstrated. We investigated the transmission characteristics of CSPR, signal power, and protection interval on seven-core fiber. The maximum penalty of CSPR is 2.1 dB at the HD-FEC threshold. The core transmission performance shows primarily a dependence by crosstalk and losses of different cores. The performance gap between the cores shows a differentiation with the change of signal power. We predict that this is related to the resulting power of XT, nonlinearity, and amplifier noise. Moreover, XT-MIMO-Volterra is proposed to reduce inter-core crosstalk and nonlinear degradation. Compared with the MIMO-Volterra and SISO-Volterra algorithms, CSPR can be reduced by 0.7 dB and 1.3 dB, respectively, and the received power gain of XT-MIMO-Volterra algorithm is improved by 0.5 dB and 0.7 dB, respectively. In this

paper, the crosstalk level of the short-reach MCF link is relatively low, and the XT-MIMO-Volterra equalizer can be verified in the long-haul link in the future.

Author Contributions: Conceptualization, F.T.; methodology, C.W.; software, T.W. and C.W.; validation, F.T., T.W. and C.Y.; formal analysis, C.Y.; investigation, C.Y.; resources, C.W.; data curation, M.Y., C.W. and T.W.; writing—original draft preparation, C.W. and T.W.; writing—review and editing, T.W., M.Y. and F.T.; visualization, T.W., F.W. and R.G.; supervision, F.T., Q.T. and Z.L.; project administration, F.T., Q.Z. and X.X.; funding acquisition, F.T. All authors have read and agreed to the published version of the manuscript.

Funding: This research was funded by the National Key R&D Program of China under grant number 2018YFB1800900, in part by the National Natural Science Foundation of China (NSFC) under Grants 62021005, 62027819, and the joint fund project of the Ministry of Education for equipment advance research under Grants 8091B032133.

Institutional Review Board Statement: Not applicable.

Informed Consent Statement: Not applicable.

Data Availability Statement: Data underlying the results presented in this paper are not publicly available at this time but may be obtained from the authors upon reasonable request.

Conflicts of Interest: The authors declare no conflict of interest.

Appendix A

The update equation of the RLS algorithm can be obtained as

$$\boldsymbol{w}_{ij}^{'}(k) = \boldsymbol{w}_{ij}^{'}(k-1) + \frac{\boldsymbol{R}_{D,i}^{-1}(k-1)\boldsymbol{y}_i(k)}{\lambda + \boldsymbol{y}_i^T(k)\boldsymbol{R}_{D,i}^{-1}(k-1)\boldsymbol{y}_i(k)}\boldsymbol{\varepsilon}_i(k). \tag{A1}$$

Let $G(k) = \frac{\boldsymbol{R}_{D,i}^{-1}(k-1)\boldsymbol{y}_i(k)}{\lambda+\boldsymbol{y}_i^T(k)\boldsymbol{R}_{D,i}^{-1}(k-1)\boldsymbol{y}_i(k)}\boldsymbol{\varepsilon}_i(k)$, we have

$$\begin{aligned}\boldsymbol{w}_{ij}^{'}(k) =& \boldsymbol{w}_{ij}^{'}(k-1) + \boldsymbol{G}(k)\\ =& \boldsymbol{w}_{ij}^{'}(k-2) + \boldsymbol{G}(k-1) + \boldsymbol{G}(k)\\ &\cdots\\ =& \boldsymbol{w}_{ij}^{'}(0) + \boldsymbol{G}(1) + \ldots + \boldsymbol{G}(k-1) + \boldsymbol{G}(k).\end{aligned} \tag{A2}$$

On the other hand, since $XT_{opt,ij}(k)$ represents the relationship between the crosstalk levels among the cores, we approximate $C_{ij}(k)$ with $XT_{opt,ij}(k)$. Given the received signal, the inverse matrix of the $\boldsymbol{XT}_{opt}(k)$ is required to estimate the transmitted signal, as shown in (20). Taking into account the memory effect, (20) is extended as

$$\begin{aligned}\boldsymbol{w}(k) =& \begin{bmatrix} XT_{opt,11}^{'}(k)\boldsymbol{w}_{11}^{'}(k) & XT_{opt,12}^{'}(k)\boldsymbol{w}_{12}^{'}(k) & \ldots & XT_{opt,1m}^{'}(k)\boldsymbol{w}_{1m}^{'}(k) \\ XT_{opt,21}^{'}(k)\boldsymbol{w}_{21}^{'}(k) & XT_{opt,22}^{'}(k)\boldsymbol{w}_{21}^{'}(k) & \ldots & XT_{opt,2m}^{'}(k)\boldsymbol{w}_{2m}^{'}(k) \\ \cdots & \cdots & \cdots & \cdots \\ XT_{opt,m1}^{'}(k)\boldsymbol{w}_{m1}^{'}(k) & XT_{opt,m2}^{'}(k)\boldsymbol{w}_{m2}^{'}(k) & \ldots & XT_{opt,mm}^{'}(k)\boldsymbol{w}_{mm}^{'}(k) \end{bmatrix}\\ =& \begin{bmatrix} \boldsymbol{w}_{11}(k) & \boldsymbol{w}_{12}(k) & \ldots & \boldsymbol{w}_{1m}(k) \\ \boldsymbol{w}_{21}(k) & \boldsymbol{w}_{22}(k) & \ldots & \boldsymbol{w}_{2m}(k) \\ \cdots & \cdots & \cdots & \cdots \\ \boldsymbol{w}_{m1}(k) & \boldsymbol{w}_{m2}(k) & \ldots & \boldsymbol{w}_{mm}(k) \end{bmatrix},\end{aligned} \tag{A3}$$

$\boldsymbol{w}(k)$ is the filter tap with crosstalk term. Bringing (A2) into $\boldsymbol{w}(k)$ gives

$$\begin{aligned}\boldsymbol{w}_{ij}(k) =& XT'_{opt,ij}(k-1)\boldsymbol{w}'_{ij}(k-1) + XT'_{opt,ij}(k)\boldsymbol{G}(k)\\ =& XT'_{opt,ij}(k-2)\boldsymbol{w}'_{ij}(k-2) + XT'_{opt,ij}(k-1)\boldsymbol{G}(k-1) + XT'_{opt,ij}(k)\boldsymbol{G}(k)\\ &\cdots\\ =& XT'_{opt,ij}(0)\boldsymbol{w}'_{ij}(0) + XT'_{opt,ij}(1)\boldsymbol{G}(1) + \ldots + XT'_{opt,ij}(k-1)\boldsymbol{G}(k-1) + XT'_{opt,ij}(k)\boldsymbol{G}(k)\end{aligned} \tag{A4}$$

We let $XT'_{opt,ij}(0)\boldsymbol{w}'_{ij}(0) \approx \boldsymbol{w}'_{ij}(0)$, i.e., the initialization of the taps is unchanged. Then,

$$\begin{aligned}\boldsymbol{w}_{ij}(k) \approx& \boldsymbol{w}'_{ij}(0) + XT'_{opt,ij}(1)\boldsymbol{G}(1) + \ldots + XT'_{opt,ij}(k-1)\boldsymbol{G}(k-1) + XT'_{opt,ij}(k)\boldsymbol{G}(k)\\ =& \boldsymbol{w}_{ij}(1) + XT'_{opt,ij}(2)\boldsymbol{G}(2) + \ldots + XT'_{opt,ij}(k-1)\boldsymbol{G}(k-1) + XT'_{opt,ij}(k)\boldsymbol{G}(k)\\ &\cdots\\ =& \boldsymbol{w}_{ij}(k-1) + XT'_{opt,ij}(k)\boldsymbol{G}(k)\\ =& \boldsymbol{w}_{ij}(k-1) + XT'_{opt,ij}(k)\frac{\boldsymbol{R}^{-1}_{D,i}(k-1)\boldsymbol{y}_i(k)}{\lambda + \boldsymbol{y}^T_i(k)\boldsymbol{R}^{-1}_{D,i}(k-1)\boldsymbol{y}_i(k)}\boldsymbol{\varepsilon}_i(k).\end{aligned} \tag{A5}$$

References

1. Cisco, U. *Cisco Annual Internet Report (2018–2023) White Paper*; Cisco: San Jose, CA, USA, 2020.
2. Wang, F.; Yao, H.; Wang, J.; Mai, T.; Xin, X.; Guizani, M. Hybrid optical-electrical data center networking: Challenges and solutions for bandwidth resource optimization. *IEEE Commun. Mag.* **2022**, *60*, 90–96. [CrossRef]
3. Chai, F.; Zhang, Q.; Yao, H.; Xin, X.; Gao, R.; Guizani, M. Joint Multi-task Offloading and Resource Allocation for Mobile Edge Computing Systems in Satellite IoT. *IEEE Trans. Veh. Technol.* **2023**, *72*, 7783–7795. [CrossRef]
4. Richardson, D.J.; Fini, J.M.; Nelson, L.E. Space-division multiplexing in optical fibres. *Nat. Photonics* **2013**, *7*, 354–362. [CrossRef]
5. Saridis, G.M.; Alexandropoulos, D.; Zervas, G.; Simeonidou, D. Survey and evaluation of space division multiplexing: From technologies to optical networks. *IEEE Commun. Surv. Tutor.* **2015**, *17*, 2136–2156. [CrossRef]
6. Puttnam, B.J.; Rademacher, G.; Luís, R.S. Space-division multiplexing for optical fiber communications. *Optica* **2021**, *8*, 1186–1203. [CrossRef]
7. Zhou, S.; Liu, X.; Gao, R.; Jiang, Z.; Zhang, H.; Xin, X. Adaptive Bayesian neural networks nonlinear equalizer in a 300-Gbit/s PAM8 transmission for IM/DD OAM mode division multiplexing. *Opt. Lett.* **2023**, *48*, 464–467. [CrossRef] [PubMed]
8. Zhu, L.; Yao, H.; Chang, H.; Tian, Q.; Zhang, Q.; Xin, X.; Yu, F.R. Adaptive Optics for Orbital Angular Momentum-Based Internet of Underwater Things Applications. *IEEE Internet Things J.* **2022**, *9*, 24281–24299. [CrossRef]
9. Zhang, J.; Liu, J.; Lin, Z.; Liu, J.; Shen, L.; Yu, S. Nonlinearity-aware adaptive bit and power loading DMT transmission over low-crosstalk ring-core fiber with mode group multiplexing. *J. Light. Technol.* **2020**, *38*, 5875–5882. [CrossRef]
10. Tan, H.; Deng, J.; Zhao, R.; Wu, X.; Li, G.; Huang, L.; Liu, J.; Cai, X. A free-space orbital angular momentum multiplexing communication system based on a metasurface. *Laser Photonics Rev.* **2019**, *13*, 1800278. [CrossRef]
11. Liu, J.; Zhu, G.; Zhang, J.; Wen, Y.; Wu, X.; Zhang, Y.; Chen, Y.; Cai, X.; Li, Z.; Hu, Z.; et al. Mode division multiplexing based on ring core optical fibers. *IEEE J. Quantum Electron.* **2018**, *54*, 1–18. [CrossRef]
12. Zhu, G.; Hu, Z.; Wu, X.; Du, C.; Luo, W.; Chen, Y.; Cai, X.; Liu, J.; Zhu, J.; Yu, S. Scalable mode division multiplexed transmission over a 10-km ring-core fiber using high-order orbital angular momentum modes. *Opt. Express* **2018**, *26*, 594–604. [CrossRef] [PubMed]
13. Zhu, B. SDM Fibers for Data Center Applications. In Proceedings of the 2019 Optical Fiber Communications Conference and Exhibition (OFC), San Diego, CA, USA, 3–7 March 2019; p. M1F.4.
14. Butler, D.L.; Li, M.J.; Li, S.; Geng, Y.; Khrapko, R.R.; Modavis, R.A.; Nazarov, V.N.; Koklyushkin, A.V. Space division multiplexing in short reach optical interconnects. *J. Light. Technol.* **2016**, *35*, 677–682. [CrossRef]
15. Qian, D.; Ip, E.; Huang, M.F.; Li, M.J.; Dogariu, A.; Zhang, S.; Shao, Y.; Huang, Y.K.; Zhang, Y.; Cheng, X.; et al. 105 Pb/s Transmission with 109 b/s/Hz Spectral Efficiency using Hybrid Single-and Few-Mode Cores. In Proceedings of the Frontiers in Optics, Rochester, NY, USA, 14–18 October 2012; p. FW6C.3.
16. Kong, D.; Jørgensen, A.; Henriksen, M.; Klejs, F.; Ye, Z.; Helgason, Ò.; Hansen, H.; Hu, H.; Yankov, M.; Forchhammer, S.; et al. Single dark-pulse kerr comb supporting 1.84 Pbit/s transmission over 37-core fiber. In Proceedings of the CLEO: QELS_Fundamental Science, Washington, DC, USA, 10–15 May 2020; p. JTh4A.7.
17. Hayashi, T.; Nagashima, T.; Morishima, T.; Saito, Y.; Nakanishi, T. Multi-core fibers for data center applications. In Proceedings of the 45th European Conference on Optical Communication (ECOC 2019), Dublin, Germany, 22–26 September 2019; pp. 1–4.
18. Le, S.T.; Schuh, K.; Tan, H.N. A closed-form expression for direct detection transmission systems with Kramers-Kronig receiver. *IEEE Photonics Technol. Lett.* **2018**, *30*, 2048–2051. [CrossRef]

19. Zhong, K.; Zhou, X.; Huo, J.; Yu, C.; Lu, C.; Lau, A.P.T. Digital signal processing for short-reach optical communications: A review of current technologies and future trends. *J. Light. Technol.* **2018**, *36*, 377–400. [CrossRef]
20. Mecozzi, A.; Antonelli, C.; Shtaif, M. Kramers–Kronig coherent receiver. *Optica* **2016**, *3*, 1220–1227. [CrossRef]
21. Liu, Y.; Li, Y.; Song, J.; Yue, L.; Zhou, H.; Luo, M.; He, Z.; Qiu, J.; Zuo, Y.; Li, W.; et al. Transmission of a 112-Gbit/s 16-QAM over a 1440-km SSMF with parallel enabled by an overlap approach and bandwidth compensation. *Opt. Express* **2021**, *29*, 8117–8129. [CrossRef]
22. Mecozzi, A.; Antonelli, C.; Shtaif, M. Kramers–Kronig receivers. *Adv. Opt. Photonics* **2019**, *11*, 480–517. [CrossRef]
23. Luís, R.S.; Rademacher, G.; Puttnam, B.J.; Awaji, Y.; Wada, N. Long distance crosstalk-supported transmission using homogeneous multicore fibers and SDM-MIMO demultiplexing. *Opt. Express* **2018**, *26*, 24044–24053. [CrossRef]
24. Fontaine, N.K.; Doerr, C.R.; Mestre, M.A.; Ryf, R.R.; Winzer, P.J.; Buhl, L.L.; Sun, Y.; Jiang, X.; Lingle, R. Space-division multiplexing and all-optical MIMO demultiplexing using a photonic integrated circuit. In Proceedings of the OFC/NFOEC, Los Angeles, CA, USA, 4–6 March 2012; pp. 1–3.
25. Randel, S.; Corteselli, S.; Badini, D.; Pilori, D.; Caelles, S.; Chandrasekhar, S.; Gripp, J.; Chen, H.; Fontaine, N.K.; Ryf, R.; et al. First real-time coherent MIMO-DSP for six coupled mode transmission. In Proceedings of the 2015 IEEE Photonics Conference (IPC), Reston, VA, USA, 4–8 October 2015; pp. 1–2.
26. Beppu, S.; Igarashi, K.; Kikuta, M.; Soma, D.; Nagai, T.; Saito, Y.; Takahashi, H.; Tsuritani, T.; Morita, I.; Suzuki, M. Weakly coupled 10-mode-division multiplexed transmission over 48-km few-mode fibers with real-time coherent MIMO receivers. *Opt. Express* **2020**, *28*, 19655–19668. [CrossRef]
27. Luis, R.S.; Puttnam, B.J.; Rademacher, G.; Awaji, Y.; Wada, N. On the use of high-order MIMO for long-distance homogeneous single-mode multicore fiber transmission. In Proceedings of the 2017 European Conference on Optical Communication (ECOC), Gothenburg, Sweden, 17–21 September 2017; pp. 1–3.
28. Shibahara, K.; Mizuno, T.; Lee, D.; Miyamoto, Y. Advanced MIMO signal processing techniques enabling long-haul dense SDM transmissions. *J. Light. Technol.* **2017**, *36*, 336–348. [CrossRef]
29. Chen, X.; Antonelli, C.; Chandrasekhar, S.; Raybon, G.; Mecozzi, A.; Shtaif, M.; Winzer, P. Kramers–Kronig receivers for 100-km datacenter interconnects. *J. Light. Technol.* **2018**, *36*, 79–89. [CrossRef]
30. Mecozzi, A. A necessary and sufficient condition for minimum phase and implications for phase retrieval. *arXiv* **2016**, arXiv:1606.04861.
31. Antonelli, C.; Shtaif, M.; Mecozzi, A. Modeling of nonlinear propagation in space-division multiplexed fiber-optic transmission. *J. Light. Technol.* **2015**, *34*, 36–54. [CrossRef]
32. Chen, X.; Chandrasekhar, S.; Randel, S.; Gu, W.; Winzer, P. Experimental quantification of implementation penalties from limited ADC resolution for Nyquist shaped higher-order QAM. In Proceedings of the 2016 Optical Fiber Communications Conference and Exhibition (OFC), Anaheim, CA, USA, 20–24 March 2016; p. W4A.3.
33. Zhang, J.; Yu, J.; Li, X.; Wei, Y.; Wang, K.; Zhao, L.; Zhou, W.; Kong, M.; Pan, X.; Liu, B.; et al. 100 Gbit/s VSB-PAM-n IM/DD transmission system based on 10 GHz DML with optical filtering and joint nonlinear equalization. *Opt. Express* **2019**, *27*, 6098–6105. [CrossRef]
34. Mathews, V.J.; Lee, J. A fast recursive least-squares second order Volterra filter. In Proceedings of the ICASSP-88, International Conference on Acoustics, Speech, and Signal Processing, New York, NY, USA, 11–14 April 1988; pp. 1383–1384.

Disclaimer/Publisher's Note: The statements, opinions and data contained in all publications are solely those of the individual author(s) and contributor(s) and not of MDPI and/or the editor(s). MDPI and/or the editor(s) disclaim responsibility for any injury to people or property resulting from any ideas, methods, instructions or products referred to in the content.